THREE-DIMENSIONAL NUMERICAL HYDRODYNAMIC SIMULATION OF ON- AND OFF-STATES IN MICROQUASARS AND QUASARS

V.V. Nazarenko, S.V. Nazarenko

Astronomical Observatory, Odessa National University,
Odessa, Ukraine, *astro@paco.odessa.ua*

ABSTRACT. As is shown in the present computations performed using three-dimensional numerical astrophysical methods, in microquasars in the course of precession of the accretion disc blown by the donor's wind the on- and off-states start being generated in the disc. In our case, the transition between these states takes 30-40 minutes of the orbital time. In the off-state the temperature changes discretely, i.e. such a change appears as separate sharp peaks, which almost merge with each other over time.

Key words: Stars: close binary system; microquasars; quasars.

1. Introduction

The present study carried out using numerical methods for astrophysics aims to show that in microquasars in the course of precession of the accretion disc blown by the donor star's wind the on-states (high/soft) and off-states (low/hard) start being generated in the disc.

The afore-mentioned phenomenon was simulated by the example of a microquasar in the semi-detached close binary (CB) Cyg -1.

The main purpose of these computations is to simulate the accretion disc and its driven precession provided that the donor slightly overfills its Roche lobe (the donor's photospheric layers are in the vicinity of the L_1 point), and the radiation wind flows from the remaining part of the donor's surface (except the vicinity of the L_1 point) at that.

2. The numerical algorithm

The numerical approach for the accretion disc formation in the microquasar Cyg X-1 is identical to that one used in massive X-ray CB and microquasar candidates Cen -3 and LMC -3 [1,2]. When computing the gas flow, the astrophysical version of the large-particle method by Belotserkovskii & Davydov [3] was applied for integration of the non-stationary Euler equations.

To show how the computations were performed, let us describe the numerical scheme of the astrophysical version of the Belotserkovskii & Davydov large-particle method. To carry out computations by the method of large particles, the entire computational domain is divided into three-dimensional rectangular grid cells, and all integer values of physical quantity indices correspond to the grid cells geometric centres. All physical quantities are constant within a given cell. The fractional indices fall at the grid cell's boundaries. The formulae below are written in such a way that the direction of an increase in each index along all three axes coincides with the positive directions of those axes. In the presented formulae the variables $U^n_{i,j,k}$, $V^n_{i,j,k}$ and $UZ^n_{i,j,k}$ are initial velocities at a given n^{th} time-step along the x, y and z axes in the cell with indices i, j and k, respectively; and the variables $U^n_{1,i,j,k}$, $V^n_{1,i,j,k}$ and $UZ^n_{1,i,j,k}$ are final velocities in the first stage of computations.

It should be noted that in the first stage of computations with a given time-step the pressure and external field effects were the only factored in. The effects of the transfer of physical quantities across the cell boundaries were accounted for in the second stage of computations. In equations 2, 7 and 9, among all non-inertial forces, only those proportional to ω_0 and ω_0^2 are taken into account; while the effects proportional to $\omega_p \cdot AA$ and $(\omega_p \cdot AA)^2$, i.e. effects associated with the donor's precession, are not factored in due to their apparent smallness as $\omega_p = \omega_0/2.56$ and $AA = 0.15$. It is also should be mentioned that the pressure effects written as the central differences in the equations below make the numerical scheme unstable; however, the effects of the physical quantity transfer, which account for the gas flow direction, are used in the second stage of computations, and that makes the numerical scheme of the large-particle method absolutely stable, steady and strictly conservative.

$$U^n_{1,i,j,k} = U^n_{i,j,k} + A \cdot dt \quad , where \tag{1}$$

$$A = \frac{P^n_{i+1/2,j,k} - P^n_{i-1/2,j,k}}{\rho^n_{i,j,k} \cdot dx_i} + \\ + \frac{GM_{donor}(x - x_{donor})}{R^3_{donor}} + \frac{GM_x(x - x_{accr})}{R^3_{accr}} - \\ - 2 \cdot V^n_{i,j,k} \cdot \omega_0 \cdot \cos\beta + \omega_0^2 (x - x_{c.m}) \cos\beta \quad (2)$$

$$\beta = \arctan z_{accr} \quad , \quad (3)$$

where $z_{accr} = AA \sin(\omega_p t)$, $\omega_p = \frac{2\pi}{P_{prec}}$, $\omega_0 = \frac{2\pi}{P_0}$, $AA = 0.15$

$$R_{donor} = \sqrt{(x - x_{donor})^2 + (y - y_{donor})^2 + (z - z_{donor})^2} \quad (4)$$

$$R_{accr} = \sqrt{(x - x_{accr})^2 + (y - y_{accr})^2 + (z - z_{accr})^2} \quad (5)$$

$$V^n_{1,i,j,k} = V^n_{i,j,k} + B \cdot dt \quad , where \quad (6)$$

$$B = \frac{P^n_{i,j+1/2,k} - P^n_{i,j-1/2,k}}{\rho^n_{i,j,k} \cdot dy_j} + \\ + \frac{GM_{donor}(y - y_{donor})}{R^3_{donor}} + \frac{GM_{accr}(y - y_{accr})}{R^3_{accr}} + \\ + 2U^n_{i,j,k} \cdot \omega_0 \cdot \cos\beta + \\ + 2UZ^n_{i,j,k} \cdot \omega_0 \cdot \sin\beta + \omega_0^2 (y - y_{c.m.}) \quad (7)$$

$$UZ^n_{1,i,j,k} = UZ^n_{i,j,k} + C \cdot dt \quad , where \quad (8)$$

$$C = \frac{P^n_{i,j,k+1/2} - P^n_{i,j,k-1/2}}{\rho^n_{i,j,k} \cdot dz_k} + \\ + \frac{GM_{donor} \cdot (z - z_{donor})}{R^3_{donor}} + \frac{GM_{accr}(z - z_{accr})}{R^3_{accr}} + \\ + 2\omega_0 \cdot V^n_{i,j,k} \cdot \sin\beta + \omega_0^2 (z - z_{c.m.}) \sin\beta \quad (9)$$

$$E^n_{1,i,j,k} = E^n_{i,j,k} + D \cdot dt \quad , where \quad (10)$$

$$D = \frac{P^n_{i,j,k}}{\rho^n_{i,j,k}} \cdot \frac{U^n_{i+1/2,j,k} - U^n_{i-1/2,j,k}}{dx_i} + \\ + \frac{P^n_{i,j,k}}{\rho^n_{i,j,k}} \cdot \frac{V^n_{i,j+1/2,k} - V^n_{i,j-1/2,k}}{dy_j} + \\ + \frac{P^n_{i,j,k}}{\rho^n_{i,j,k}} \cdot \frac{UZ^n_{i,j,k+1/2} - UZ^n_{i,j,k-1/2}}{dz_k} \quad (11)$$

$$P^n_{i,j,k} = n^n_{i,j,k} \cdot KT^n_{i,j,k} \quad (12)$$

In the presented formulae G - the constant of gravitation; M_{donor} and M_{accr} - the donor and accretor masses, respectively; x_{donor}, y_{donor}, z_{donor} - the donor's geometric centre coordinates; x_{accr}, y_{accr}, z_{accr} - the accretor's geometric centre coordinates; P_0 - the orbital period; P_{prec} - the precession period of the target CB; $x_{c.m.}$, $y_{c.m.}$, $z_{c.m.}$ - the coordinates of the CB centre of mass; $E^n_{i,j,k}$ - specific internal energy at the beginning of a given time-step in the grid cell with indices i, j, k, $E^n_{1,i,j,k}$ - specific internal energy at the end of the first stage of the n^{th} time-step in the grid cell with indices i, j, k; $\rho^n_{i,j,k}$ - the density in the first stage of the n^{th} time-step in the grid cell with indices i, j, k; dx_i, dy_j, dz_k a given grid cell's dimensions in the x, y, z directions; $P^n_{i,j,k}$ - the pressure in the grid cell with indices i, j, k at the n^{th} time-step; K - the Boltzmann constant; $T^n_{i,j,k}$ - the temperature in the grid cell with indices i, j, k at the n^{th} time-step. The physical quantities with fractional indices were computed with numerical differences of up to and including the third order that resulted in rather accurate calculation of the physical quantities on the non-uniform computational grid.

The second stage of computations of the numerical algorithm for the large-particle method is described starting with formula 13. In this stage the flows of physical quantities across the grid cell boundaries are computed, and the final velocities and temperatures at a given time-step are determined. Formula 13 describes the calculation of change in density at a given time-step in a given grid cell. Formulae 14-15 describe calculations of the mass flow across $i - 1/2$ boundary of a given grid cell. As is seen in these formulae, the velocity directions are taken into account when computing the mass flow. Such arrangement of the second stage computations for the large-particle method makes the scheme integrally stable, steady and strictly conservative. The other mass flows across other grid cells boundaries, used in formula 13, are computed similarly to formulae 14 and 15. At that the positive direction of the velocity in formulae 14 and 15 corresponds to the increment in the grid cell number.

$$\rho^{n+1}_{i,j,k} = \rho^n_{i,j,k} + \frac{\triangle M^n_{i-1/2,j,k} - \triangle M^n_{i+1/2,j,k}}{dx_i dy_j dz_k} + \\ + \frac{\triangle M^n_{i,j-1/2,k} - \triangle M^n_{i,j+1/2,k}}{dx_i dy_j dz_k} + \\ + \frac{\triangle M^n_{i,j,k-1/2} - \triangle M^n_{i,j,k+1/2}}{dx_i dy_j dz_k} \quad (13)$$

$$\triangle M^n_{i-1/2,j,k} = dy_j \cdot dz_k \cdot U^n_{1,i-1/2,j,k} \cdot \rho^n_{i-1,j,k} \cdot dt, \\ if \ \mathrm{U}^n_{1,i-1/2,j,k} > 0 \quad (14)$$

$$\triangle M^n_{i-1/2,j,k} = dy_j \cdot dz_k \cdot U^n_{1,i-1/2,j,k} \cdot \rho^n_{i,j,k} \cdot dt, \quad if\ \mathrm{U}^n_{1,i-1/2,j,k} < 0 \tag{15}$$

When computing formula 18, three velocity components (calculated in the first stage) and total energy, which are determined in curly brackets in formula 16, successively substitute for the variable $Z^{n+1}_{i,j,k}$.

$$Z^{n+1}_{i,j,k} = \left\{U^n_{1,i,j,k}; V^n_{1,i,j,k}; UZ^n_{1,i,j,k}; E^n_{total,i,j,k}\right\} \tag{16}$$

$$E^n_{total,i,j,k} = \frac{(U^n_{1,i,j,k})^2 + (V^n_{1,i,j,k})^2}{2} + \frac{(UZ^n_{1,i,j,k})^2}{2} + E^n_{1,i,j,k} \tag{17}$$

$$Z^{n+1}_{i,j,k} = \frac{Z^n_{i,j,k}\rho^n_{i,j,k}}{\rho^{n+1}_{i,j,k}} + \frac{\triangle M^n_{i-1/2,j,k} \cdot Z^n_{i-1,j,k}}{\rho^{n+1}_{i,j,k} \cdot dx_i \cdot dy_j \cdot dz_k} + \frac{-\triangle M^n_{i+1/2,j,k} \cdot Z^n_{i,j,k} + \triangle M^n_{i,j-1/2,k} \cdot Z^n_{i,j-1,k}}{\rho^{n+1}_{i,j,k} \cdot dx_i \cdot dy_j \cdot dz_k} + \frac{-\triangle M^n_{i,j+1/2,k} \cdot Z^n_{i,j,k} + \triangle M^n_{i,j,k-1/2} \cdot Z^n_{i,j,k-1}}{\rho^{n+1}_{i,j,k} \cdot dx_i \cdot dy_j \cdot dz_k} - \frac{\triangle M^n_{i,j,k+1/2} \cdot Z^n_{i,j,k}}{\rho^{n+1}_{i,j,k} \cdot dx_i \cdot dy_j \cdot dz_k} \tag{18}$$

The boundary conditions and radiation wind from the donor in these computations are similar to those ones in our earlier studies [1, 2].

We assumed that the binary parameters are as follows: the Cyg X-1 orbital period is 5.6 days; the accretor's mass is 10 $M_\odot$; the donor's mass is 20 $M_\odot$[4]; the accretion velocity in the disc is about $3.0 \cdot 10^{-8}$ $M_\odot$/year [5].

The condition of the accretion disc formation is that the wind acceleration in the radial direction in the vicinity of the L_1 point and along the line of centres in the accretor's Roche lobe should decrease to zero. The L_1 point vicinity starts at the L_1 point and extends to the accretor's Roche lobe; in these computations the chosen vicinity extension in the radial direction is 0.22 (here and elsewhere all distances are given in units of orbital separation).

In this study, the driven precession computations were performed given that the precession donor is embedded, i.e. fixed in this computational grid while it is accretor that changes its position in space (i.e. moves across the computational grid). However, mutual positioning of the accretor and donor changes in a similar way as if it is the donor is precessing (the effect of the uniform motion relativity in classical physics). At that we assume that the donor is precessing uniformly without surges and accelerations, so the accretor's motion will be uniform as well. The precession period is assumed equal to 20 orbital periods.

It should be noted that we do not assume any additional conditions for the on- and off-states creation, they should be generated in the disc under the only effect of precession with no additional conditions.

3. The computational results of the on- and off-states generation in the disc

The study task is posed in such a way that the initiation of the winds from the donor and accretion disc is calculated first, then the accretion disc's driven precession is started, and the computations proceed as far as the computer capability permits to trace disc's evolution as long as possible.

The donor's wind is initiated during the first quarter-third of the first orbital period, and the disc is formed in the course of the first orbital period.

The orbital plane section and that one of the plane, which is perpendicular to it and lies on the line of centres, in the computational domain at the instant of time corresponding to the precession period 1.31 are presented in Fig. 1 and 2. These figures show the donor, wind from donor and accretion disc, which is tightly compressed by the wind from the donor at the given precession phase (the beginning of the low/hard phase).

The key properties of the disc resulted from these computations, such as the temperature in the disc's centre and accretion rate around the disc's centre as functions of time, are shown in Fig. 3 and 4. As is seen in these figures, the accretion rate and temperature over each precession period change markedly (by more than two orders of magnitude); when there is a two-order increase in the temperature in the disc's centre, the accretion rate drops accordingly by two or just over two orders of magnitude at the same instants. All those variables fluctuate dramatically at that while the transition between high and low temperature conditions, and low and high accretion rates, respectively, takes 30-40 minutes of the orbital time.

Thus we can state the fact that in our computations in the course of precession of the numerical disc model high and low temperature conditions, and low and high accretion rates, respectively, are generated; and we interpret these conditions as the off- and on-states of the accretion discs in microquasars, respectively. The fact that the numerical disc model alters significantly over the precession period is given in Fig. 5 where it is shown that the disc's mass changes with the precession period (the disc's mass is given on the logarithmic scale in $M_\odot$). As it is seen in this figure, the disc's mass

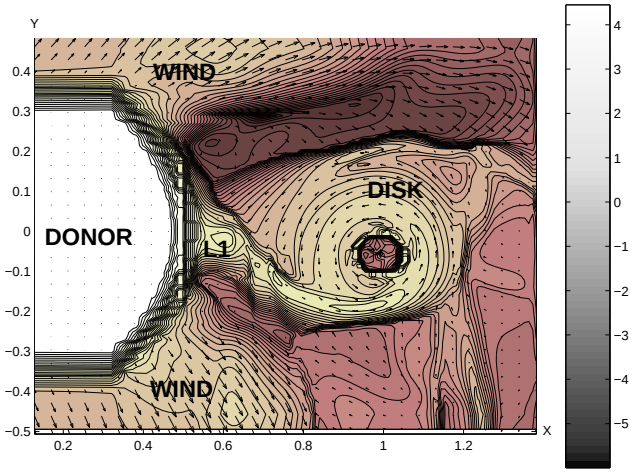

Figure 1: The number density distribution over the computational domain at the precession phase 1.31 in the orbital plane.

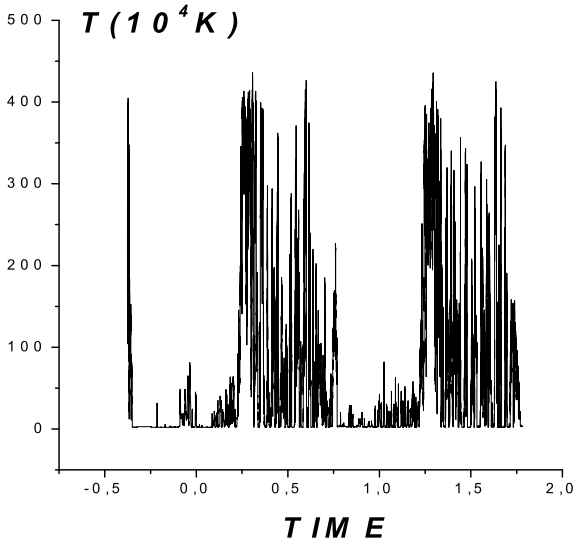

Figure 3: The temperature in the disc's centre over time.

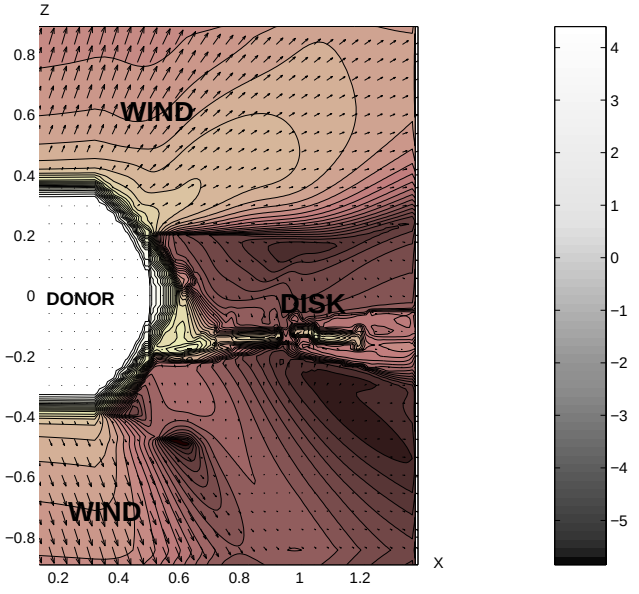

Figure 2: The number density distribution over the computational domain at the precession phase 1.31 in the Z-X plane.

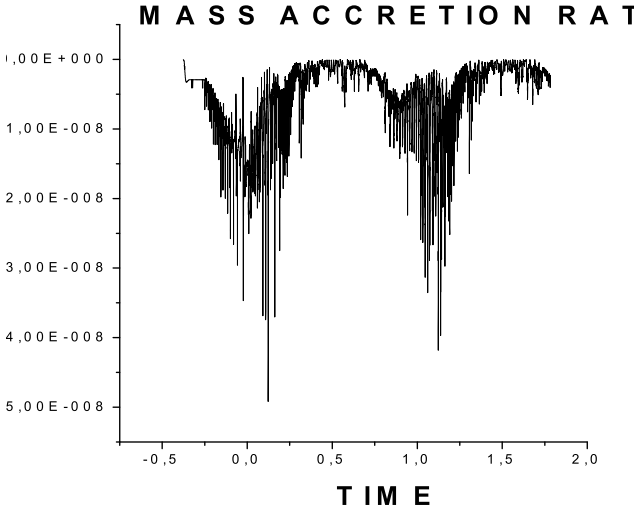

Figure 4: The mass accretion rate in the disc's centre over time.

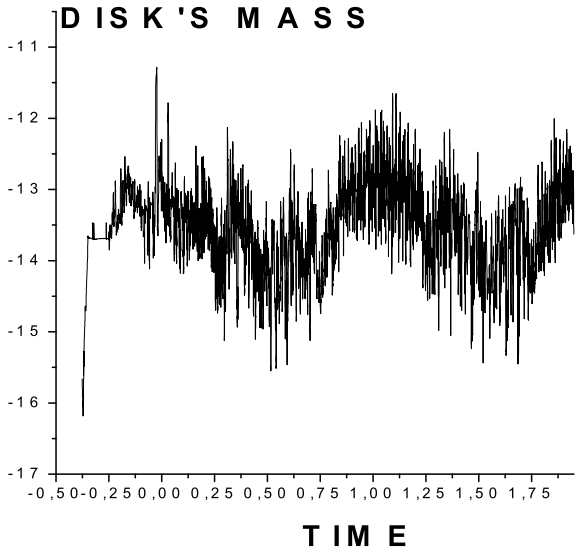

Figure 5: The disc's mass over time on the logarithmic scale in $M_\odot$.

changes by almost two orders of magnitude; and at that when the accretion rate is maximum at the high/soft phase, the disc's mass also reaches maximum.

As can be concluded from the aforesaid, the precession mechanism of the on- and off-states generation works as follows: while the accretion disc is precessing, the wind from the donor flows onto the disc at different instants at various angles, causing the disc's tight compression (that occurs near the precession phase 0.00, which is approximately the middle of the high/soft phase); in that case the accretion rate increases, and the on-state occurs in the disc as the radiative cooling is very effective with high concentrations in the disc's centre, and hence the gas cools down to low temperatures. At the counter precession phase near the phase 0.50 (which is approximately the middle of the low/hard phase) the disc does not practically experience the wind's pressure that results in the wind-accretion rate decrease and the off- state occurrence as the radiative cooling becomes ineffective at that instant, and the temperature in the disc's centre increases significantly.

4. Conclusions

This study conducted using methods for three-dimensional numerical hydrodynamics shows that in microquasars in the course of precession of the accretion disc blown by the donor's wind the on- and off-states are generated in the disc, at that the transition between these states is catastrophically fast and takes 30-40 minutes of the orbital time. The computations also showed that the temperature in the disc's centre changes discretely in the off-state and such a change appears as separate sharp peaks, which are at very small distances from each other (5-10 minutes of the orbital time). As follows from the observations, such discrete behaviour of the temperature in the low/hard phase corresponds to the similar discrete behaviour of the hard X-rays in the low/hard phase.

References

Nazarenko V.V.: 2006, *Astronomy Reports,* **50**, 647.
Nazarenko V.V.: 2008, *Astronomy Reports,* **52**, 40.
Belotserkovskii O.M., Davydov Yu.M.: 1982, "The big particles code in gas dynamics", Moskaw, Scientist, 391.
Karitskaja E.A., Bochkarev N., private communications.
Wijers R.A.M.J. & Pringle J.E.: 1999, *MNRAS,* **308**, 207.